RSC Advances

ROYAL SOCIETY OF CHEMISTRY

www.rsc.org/advances

Gold dotted hydroxyapatite nanoparticles as multifunctional platforms for medical applications

Catarina Ferreira dos Santos[a,b], Pedro Sousa Gomes[c,d], Maria Margarida Almeida[e], Marc-Georg Willinger[f], Ralf-Peter Franke[g], Maria Helena Fernandes[c,d], Maria Elisabete Costa*[e]

[a]Department of Mechanical Engineering, Escola Superior de Tecnologia de Setúbal, Instituto Politécnico de Setúbal, Setúbal, Portugal

[b]ICEMS, Instituto Superior Técnico, Technical University of Lisbon, Av. Rovisco Pais Lisboa 1049 001, Portugal.

[c]Laboratory for Bone Metabolism and Regeneration, Faculdade de Medicina Dentária, Universidade do Porto, Portugal.

[d]MedInUP - Center for Drug Discovery and Innovative Medicines, University of Porto, Porto, Portugal

[e]Department of Materials and Ceramics Engineering, CICECO, University of Aveiro, 3810-193 Aveiro, Portugal.

[f]Max Planck Gesell, Fritz Haber Inst, Dept Inorgan Chem, D-14195 Berlin, Germany.

[g]Central Institute for Biomedical Technology, Biomaterials Division, University of Ulm, Ulm, Germany.

*corresponding author- elisabete.costa@ua.pt

Abstract

A novel synthesis approach for coupling metallic gold nanoparticles (AuNP) to the facets of hydroxyapatite crystalline nanoparticles (HapNP) without additional reducing agent was developed. Hexagonal prism-shaped hydroxyapatite nanoparticles (HapNP) were firstly precipitated by a hydrothermal route assisted by citric acid which left behind carboxylate species adsorbed on HapNP facets. HapNP were then used as templates for gold precipitation: when exposed to gold ions, the carboxylate species on HapNP prismatic facets were able to trigger the nucleation of metallic gold by reducing “in-situ” the gold ions. The used conditions didn´t allow the extensive growth of gold nuclei and hence gold dots with diameters not larger than 2.5nm were formed on HapNP facets. The obtained (Hap-AuNP) heteronanostructures combine nanoprisms of Hap, a highly biocompatible material easily recognised by the human body, with metallic nanosized gold that imparts a plasmon

resonance (SPR) effect to the synthesized nanostructures which is of great promise to be further explored in the context of thermotherapy and imaging strategies.
Human mesenchymal stem cells were exposed to a concentration range of Hap-AuNP but no cytotoxic effects from the heteronanostructures were observed. Furthermore, Hap-AuNP greatly enhanced the expression of Runx2 and ALP. These results predict the synthesized Hap-AuNP particles to be also potentially interesting for medical needs requiring nontoxic materials able of bone defect repair and furthermore skilled with SPR properties which can be potentially advantageous for therapeutic and diagnosis purposes.

1-Introduction

The unprecedented developments in materials synthesis and characterization techniques at the nanoscale are encouraging audacious approaches in matter manipulation and assembling which are being exploited for designing nanostructures with improved or new properties and functionalities as compared with their bulk counterparts. Nanomedicine is one of the multiple fields where such forefront nanotech achievements are fostering innovative strategies as is the case of cancer theranostics[1].

Gold nanoparticles (AuNP) are an emblematic example of biomedical nanostructures with a well-known Surface Plasmon Resonance effect (SPR) which frequency is affected by nanoparticles (NP) size, shape, inter-distance and refractive index of NP surrounding media. This effect has been largely exploited for labeling and probing a wide variety of biomolecules that interfere with AuNP dispersed state and with the refractive index of NP environment due to adsorption[2]. Such applications demand a close control of AuNP morphological attributes (size and shape) and, very importantly, of AuNP dispersed condition. These pre-requisites have been covered by a large volume of publications and hence different proposals for AuNP production including synthesis methods, reagents, solvents, stabilizers among others are found in recent literature. Currently AuNP are also being explored as photothermal contrast agents for cancer imaging and therapy[3,4]. Plasmonic AuNP strategically located in tumors are used to enhance near-infrared laser absorption and dissipation as heat and thus to produce a local temperature increase which disturbs cellular functions ending up on cell death. Additionally X-ray absorbing properties of AuNP can be also used for biodistribution data acquisition enabling tumor non-invasive imaging and 3D

reconstruction[3,5]. Other treatment methods exploit spherical AuNP as sensitizing agents in radio frequency ablation and X-ray radiation cancer therapies[3,6-8].

Hydroxyaptite (Hap) is an appealing inorganic biomaterial as its chemical composition, crystalline structure and particle morphology if appropriately engineered can replicate the chemical and physical attributes of the inorganic component of human bone and teeth[9,10] while offering enhanced adsorptive ability towards a considerable number of biomolecules and drugs[11,12]. Addressing the combination of AuNPs and Hap exceptional properties and benefiting from the ability of AuNPs to be easily functionalized for specific protein binding, hybrid hydroxyapatite gold nanoparticles (Hap-AuNPs) structures with a portfolio of interesting properties for various bioapplications as immunosensing[13], bone tissue regeneration[12,14,15] improvement of hemocompatibility[15,16] have been often reported. The methods found for producing and or assembling Hap-AuNPs structures are quite diverse[13-16], but very often gold and Hap particles are precipitated separately and then assembled to form the composite material[12,13,16,17]. Turkevich method[18] or a variant of it is still being the method of choice for AuNPs synthesis whereas no favourite method could be identified for Hap synthesis as multiple techniques have been successfully employed[19]. Frequently polymers are required (e.g. collagen, chitosan) as linkers or agents for coupling gold and Hap[14,15,17]. One easy method for producing uniform Hap nanoparticles (HapNP) is the hydrothermal synthesis in presence of an organic chelating ion or molecule[20-23] used as a "shape tailoring agent" that allows controlling the particle size and shape[24,25]. As recently reported, citrate ion could modulate prismatic HapNP under specific hydrothermal synthesis conditions[23].

The present study addresses the nucleation and growth of AuNP onto the surface of HapNP for producing organized composite nanostructures. The ability of citric ion to play a dual role, i.e. as HapNP tailoring agent and as *in situ* reducing reagent of Au^{3+} leading to local Au^0 nucleation and growth on HapNP facets is the engineering tool here exploited. From the application point of view, a wide potential is anticipated considering the benefits of gathering the accurate control of AuNPs size, shape and surface chemistry with the high biocompatibility of HapNP. Due to the bone affinity, biomimetic features and osteointegrity, HapNP is particularly suited for bone-related applications[26,27]. Thus, besides the interest of using AuNP as excellent contrast elements[28,29] depending on their size, the tunability of SPR is envisaged with great usefulness for imparting simultaneous imaging and therapeutic

abilities to Hap-AuNPs nanostructures making them powerful tools for differentiated bone applications. Therefore, another interest is the discussion of the potential effects of HapNP assembled with AuNPs on the proliferation and differentiation of human mesenchymal stem cells, due to their role in bone metabolism and regeneration, an issue which has not been covered so far.

2-Materials and methods

2.1- Hydroxyapatite synthesis

An hydrothermal precipitation method previously reported[30] was followed for HapNP synthesis. The starting precursors solution was prepared as follows: a 0.6M citric acid monohidratate ($C_6H_8O_7.H_2O$) (Riedel-deHaën, 99.5%) solution was mixed with a 0.2M calcium nitrate $Ca(NO_3)_24H_2O$ (Riedel-deHaën, 99%) solution and then added with a 0.2M ammonium hydrogen phosphate $(NH_4)_2HPO_4$ (Merck, 99%) solution. The pH of the solution was adjusted to 8.1 with small additions of a 25% ammonia solution (Riedel-deHaën). The final solution was poured into a 100 ml teflon vessel, filling up 50% of the total vessel volume. The teflon vessel was then sealed in a stained-steel autoclave and subsequently transferred into an oven at 180ºC where it stayed under autogeneous pressure during 24 hours. After that the autoclave was quenched in water at room temperature. Finally the precipitated particles were collected and filtered using a glass Millipore filter vessel and then dried in a desiccator.

2.2- Gold precipitation

For the precipitation of gold, 86.5 µl of a hydrogen tetracholoroaurate ($HAuCl_4$) solution were added to 500 ml of deionized water in order to obtain a $0.25x10^{-3}$ M gold solution with pH ~3. Then 25 ml of the gold solution were heated at ~100ºC for 3 minutes and subsequently added with 50 mg of HapNP which were synthesized as described in 2.1. The resulting suspension was maintained under boiling conditions during 5 minutes. The overall procedure was repeated for covering different reaction times, i.e. 10 and 20 minutes of boiling times. After that the particles (Hap-AuNP) were repeatedly washed with deionized water while being filtered with a glass Millipore filter vessel and then dried in a desiccator.

2.3-Particle characterization

The morphology of all the obtained particles by precipitation was evaluated by electron transmission microscopy (TEM) using a Hitachi H-9000-NA microscope operated at 200 kV and high resolution electron transmission microscopy (HRTEM) images were carried out on a JEOL 2200 FS microscope operating at 200 kV. For TEM analysis the particles were dispersed with 2-propanol and scattered over copper grids coated with a formvar film. TEM images were used to determine the size of AuNP. More than 100 particles were randomly counted to determine the particle size distribution using Image-J software. Particle crystalline phases were identified by powder X-ray diffraction (XRD) analysis (Rigaku PMG-VH with CuKα radiation =1.5405 Å). Fourier transform infrared spectroscopy (FTIR) was performed for identifying the functional groups, using a Mattson galaxy 3020 spectrophotometer. The test samples were prepared by mixing ~2 mg of the precipitated particles with ~300 mg of spectroscopic-grade KBr (Merck) and then shaping the mixture as a disk. The infrared spectra were recorded in transmittance mode in the region of 4000-400 cm^{-1} with a resolution of 4 cm^{-1}. The UV-vis absorption data were collected on a Shimadzu MPC-3100 PC series spectrophotometer using an auto scan between 200 and 700 nm. The specific surface area (SSA) of the obtained particles was determined by N_2 adsorption using a micromeritics – Gemini 2370 V5 equipment. The samples were thoroughly degassed at 120ºC for 24 hours before nitrogen adsorption. The SSA was determined based on the multipoint Brunauer-Emmett-Teller isotherm (BET)[20].

2.4 Interaction of Hap-AuNPs with human mesenchymal stem cells

Human Mesenchymal Stem Cells-bone marrow derived (HMSC-bm, Innoprot), according to the supplier, were found to stain positive for CD44 and CD90 – characteristic markers of the population phenotype. Third subculture cells were used to evaluate the cell response to the nanoparticles.

HMSC, 10^4 cells/cm^2, were cultured in minimum essential medium Eagle, alpha modification (α-MEM, Sigma) containing 10% foetal bovine serum (FBS, Sigma), 50 μg/ml ascorbic acid, penicillin (10 units/ml)/streptomycin (2.5 μg/ml) (P/S solution, Sciencell) and 2.5 μg/ml fungizone. After 24 hours, the medium was removed and fresh complete culture medium, containing sterilized HapNP or Hap-AuNPs - 1, 10, 100 and 500 μg/ml was added

to the adherent cells. Cultures were incubated for further 1, 3 and 7 days without any medium change. Cultures performed in the absence of nanoparticles were used as control. Incubation was carried out in a humidified atmosphere of 95% air and 5% CO_2 at 37ºC. Cultures were characterized at days 1, 3 and 7, as follows.

DNA content. DNA content was analyzed by the PicoGreen DNA quantification assay (Quant-iT™ PicoGreen® dsDNA Assay Kit, Molecular Probes Inc., Eugene), according to manufacturer´s instructions. Cultures were treated with Triton X-100 (0.1%) (Sigma) and fluorescence was measured on an Elisa reader (Synergy HT, Biotek) at wavelengths of 480 and 520 nm, excitation and emission respectively, and corrected for fluorescence of reagent blanks. The amount of DNA was calculated by extrapolating a standard curve obtained by running the assay with the given DNA standard.

Cellular viability. MTS [31] and LDH [32] assays were used to estimate cell viability. The MTS assay is based on the reduction of MTS tetrazolium compound [3-(4,5-dimethylthiazol-2-yl)-5-(3-carboxymethoxyphenyl)-2-(4-sulfophenyl)-2H-tetrazolium] to a purple formazan product by the mitochondrial reductase enzymes system on viable cells. MTS solution (Cell Titer 96® Aqueous One Solution Cell Proliferation Assay, Promega), 20 µl, was added to the culture medium (100 µl, 96-well plates), and cultures were incubated during 4 h (37ºC, in a humidified atmosphere of 95% air and 5% CO_2). The absorbance was measured at 492 nm in a ELISA reader (Synergy HT, Biotek). The lactate dehydrogenase (LDH) assay is based on the reduction of NAD by the action of LDH released to the medium due to cell damage (plasma membrane integrity) or lysis. The resulting reduced NAD (NADH) is utilized in the stoichiometric conversion of a tetrazolium dye. Determination of the total LDH was performed using the *In vitro* toxicology assay kit lactate dehydrogenase based (Sigma-Aldrich; St. Louis, MO), according to the manufacturer's instructions. The amount of LDH leakage to the medium was normalized to total LDH. Results are expressed in percent of cells viability compared to the control.

CLSM observation. Cultures were fixed (3.7% methanol-free formaldehyde, 15 min), permeabilized with 0.1% Triton, and incubated with bovine serum albumin (Sigma Aldrich), 10 mg/ml in PBS (1 h), in order to block non-specific interactions. Cytoskeleton filamentous actin (F-actin) was visualized by treating permeabilized cells with Alexa Fluor® 488-conjugated phalloidin (Invitrogen), 1:100 in PBS (20 min). Cells were counterstained with propidium iodide (Sigma Aldrich), 10 mg/ml in PBS (5 min). Stained samples were

mounted in Vectashield® (Vector laboratories) and examined in a Leica SP5 AOBS (Leica Microsystems®) microscope.

Gene expression by RT-PCR. Adherent 24-hour HMSC were exposed to 100 μg/ml HapNP or Hap-AuNPs nanoparticles for three days, and were evaluated for the expression of the housekeeping gene GAPDH (glyceraldehydes-3-phosphate dehydrogenase) and the osteoblastic genes Runt-related transcription factor 2 (RUNX-2), alkaline phosphatase (ALP), osteocalcin (OC) and osteoprotegerin (OPG). RNA was extracted using RNeasy® Mini Kit (QIAGEN) according to manufacturer's instructions. RNA was quantified by measuring the absorbance of the samples at 260 nm. RNA, 0.5 μg, was reverse transcribed and amplified (25 cycles) with the Titan One Tube RT-PCR System (Roche), with an annealing temperature of 55ºC. Table 1 show the primers used in the RT-PCR analysis. After electrophoresis on a 1% (w/V) agarose gel, the bands were analysed by densitometry with ImageJ 1.41 software. Values were normalized to the corresponding GAPDH value of each experimental condition.

ALP activity. ALP activity was evaluated in cell lysates (0.1% Triton X-100, 5 min) by the hydrolysis of *p*-nitrophenyl phosphate in alkaline buffer solution (pH~10.3; 30 min, 37 ºC) and colorimetric determination of the product (*p*-nitrophenol) at 400 nm in an ELISA plate reader (Synergy HT, Biotek). ALP activity was normalized to total protein content (quantified by Bradford's method) and expressed as nmol/min.$mg_{protein}^{-1}$.

Statistical analysis. Three independent experiments were performed; in each experiment, six replicas were set up for the biochemical assays and two replicas for the qualitative assays. Results are presented as mean ± standard deviation (SD). Groups of data were evaluated using a two-way analysis of variance (ANOVA) and no significant differences in the pattern of the cell behavior were found. Statistical differences between experimental groups were assessed by Bonferroni's method. Values of $p \leq 0.05$ were considered statistically significant.

3- Results and discussion

3.1- Synthesis of functionalized hydroxyapatite nanosized particles (HapNP)

Literature reports on hydroxyapatite synthesis methods are plentiful. The choice of a particular synthesis methodology is normally dictated by particle morphology and/or

crystallinity criteria. In the present case, a hydrothermal precipitation method previously reported [23]was selected aiming to obtain crystalline HapNP with nanometric dimensions and well-defined facets easily imaged by electron microscopy. Other issues including the surface chemistry of the precipitated particles were taken into account as well.

Figure 1a shows a picture of the HapNP as synthesized by the hydrothermal procedure. As observed the particles display a yellowish light colour. The crystalline phase composition of these particles is revealed by the XRD pattern presented in Figure 2 (curve (a)) which diffraction peaks can be assigned to hydroxyapatite (Hap) according to the JCPDS Nº 09-0432. Figure 3a shows the FT-IR spectrum of the precipitated HapNP where the characteristic peaks of hydroxyapatite are detected [33-35]. Furthermore some features attributed to organic groups are also identified in the range of 1680 to 1350 cm^{-1} (Figure 3b). The band at 1384 cm^{-1} may be ascribed to CH_2 scissoring and carboxylate groups differently coordinated to Hap surface under monodentate or bidentate configurations[6,30] may account for the bands at 1402, 1458, 1577 and 1669 cm^{-1}. Such adsorbed carboxylate species $[R\ (COO^-)_x]_{ads}$ can be interpreted as fingerprints of the original citrate ions that might have decompose under the temperature and pressure regime used for Hap synthesis, in line with the reports on citric acid thermal degradation[36-39].

The particle morphology assessed by TEM and imaged in Figure 4(a and b) can be well described by a hexagonal prismatic shape with a width (w) lying between 20 and 30 nm and a length (l) ranging from 50 to 100 nm. These nanoscale dimensions of the prismatic hydroxyapatite nanoparticles (HapNP) account for a large specific surface area of 55 m^2/g and an aspect ratio (l/w) larger than 1.7. Figure 4b shows the HRTEM image of a HapNPs where well-defined lattice fringe patterns are observed. The distance between adjacent lattice fringes corresponds to an interplanar distance of 0.65 nm that can be indexed to the d-spacing value of hydroxyapatite crystal (010) planes which are parallel to *c* axis. The used citrate-mediated hydrothermal synthesis thus favored HapNP preferential growth along the c-axis which resulted on elongated particle morphology.

The interaction of citric acid with HapNP surface and its effects on HapNP growth have been frequently addressed, from both experimental and theoretical perspectives. Calcium phosphate precursor solutions containing citric acid, have been reported to favor the precipitation of HapNP with elongated shape, under varied conditions of temperature and pressure[23]. According to computer simulations studies[33,40], a strong binding of citric acid

or of citrate ion to Hap lateral prismatic facets may slow down their growth rate and consequently enable its dominant expression on the final particle morphology. Such theoretical predictions might explain the present results assuming that citrate ions at an early stage of the hydrothermal processing and citrate derived moieties at a later stage of the precipitation perform as lateral growth inhibiters, hence contributing to shape the particles. An accurate picture of citrate role under the temperature and pressure regime of this work requires a complete follow up of the interplay of Hap nucleation, growth and citrate degradation progress which is now an ongoing study.

3.2- Templating gold precipitation with HapNP

HapNP synthesized by hydrothermal technique were used as substrate for the growth of AuNP. The effects of gold precipitation time were examined in order to assess its impact on the gold particle size and size distribution.

3.2.1- Gold particle crystal structure, morphology and SPR

Figure 1b to 1d allows following the colour evolution of the HapNP after submitted to the gold precipitation experiments during different reaction times. The original yellowish colour of HapNP gives place to a purple colour as precipitation occurs, hence anticipating the presence of nanometric sized gold particles in the Hap-AuNPs powders[19]. Further evidences of gold precipitation are provided by the XRD patterns shown in Figure 2(b to d) where the peak detected at $2\theta \sim 38^{o}$ was identified as the more intense peak of metallic gold[41] according to the JCPDS N^{o} 071-4614.

Figure 5(a and b) shows the HRTEM images of the Hap-AuNPs particles collected after different precipitation times. It is clearly observed that the prismatic HapNP previously imaged in Figure 4a, are now uniformly spotted with nanosized dark dots, which dimensions vary approximately from 1,5 to 2,5 nm as the synthesis time increases from 5 min (Figure 5a) to 20 min (Figure 5b). These are nanosized dots of metallic gold which were precipitated on HapNP facets, accounting for the HapNP colour variation previously described. It was also found that Hap-AuNPs after 20 min of reaction apparently have a lower density of larger AuNPs dots on their surfaces as documented by the particle size distribution curves (Figure 5c). This may be explained by an Ostwald ripening mechanism favouring the growth of larger AuNP at the expense of smaller ones[19]. Although the dots become larger, they

apparently preserve the spherical shape which is known to be the lowest-energy shape, often observed among metal nanoparticles obtained from metal salts reaction with reducing agents[42]. The present strategy proved to be highly reproducible, consistently coupling uniform spherical AuNP to HapNP.

Figure 6 shows the UV-vis spectra of HapNP as prepared (a) and of Hap-AuNPs after 5 min (b) and 20 min (d) of synthesis. Confirming previous reports[41] no UV-vis band is detected in the range of 300-800 nm for HapNP as prepared. Conversely, a characteristic SPR band of AuNPs is clearly observed around 550 nm in the spectra of Hap-AuNPs. The observed SPR accounts for the strong colour changes observed on the particles[29] and confirms the formation of spherical AuNP by this synthesis method, in a good agreement with TEM results. Moreover, it was observed that the SPR band is similar for the two selected precipitation times, which may be related to the small variation in particle size which is not significant to be detected by UV-Vis in powders. The SPR band shift from the well-known value of 520 nm reported for isotropic spherical gold particles (<20 nm) dispersed in water[43,44] to the value here observed of ~550nm may reflect the influence of the substrate (Hap) refractive index (1.64) which is larger than that of water (1.33), the surrounding medium usually referred[45]. A similar shifting effect was also reported for gold nanoparticles of ~5.5 nm deposited over SiO_2/Si substrates [46].

3.2.2-Mechanism of gold precipitation

The process of AuNPs growth on HapNP surface was also followed by FTIR spectra analysis aiming to assess modifications on adsorbed species. Figure 3a compares the full spectrum of HapNP as prepared with those of Hap-AuNPs collected after 5, 10 and 20 min, being the details of the carbonate region (1350-1680 cm^{-1}) magnified in Figure 3b. Although Hap characteristic features are observed in all the spectra, some differences are noticed in the 1350-1700 cm^{-1} region as gold precipitation proceeds (Figure 3b). In this spectral slot where citrate derived species containing carboxylate groups differently coordinated to HapNP surface are expected to be detected[47], some features are seen to disappear or undergo a strong intensity decrease as observed for the bands at 1384, 1567 and at 1670 cm^{-1} although the bands at 1402 cm^{-1} and 1458 cm^{-1} remain unaffected by the Au synthesis process. All together these results indicate that some adsorbed species containing COO^-

groups may be appropriately configured to participate in Au nucleation[44] whereas other groups appear to be less strategic in the metal precipitation.

As referred by S. Kumar et al.[48] gold precipitation in bulk solution by Turkevich method can be systematized according to the following steps: an initial step comprises the oxidation of citrate $(CH_2COO^-)_2C(OH)COO^-$ to an acetone dicarboxylic acid $(CH_2COO^-)_2CO$ accompanied by the reduction of auric salt ($AuCl_3$) to aurous salt (AuCl). The subsequent step requires the disproportionation of AuCl into gold atoms (Au^0) and $AuCl_3$ as schematized by the equation $3AuCl \rightarrow 2Au^0 + AuCl_3$. This last step requires various aurous chloride molecules to be in a nearby condition which is facilitated by acetone dicarboxylic species that tethers aurous chloride molecules.

In this work, gold precipitation took place on HapNP surface, most likely on the lateral prismatic faces as confirmed by TEM images. When HapNP are added to the reagent $HAuCl_4$ aqueous solution (pH~3), HapNP acquire a neutral or weakly positive zeta potential[23] which favours electrostatic attachment of negatively charged auric complexes, i.e. $[AuCl_3OH]^-$ and/or $[AuCl_2OH_2]^-$ which are abundant species in $HAuCl_4$ solution at pH 3-4[49,50]. It is here proposed that $[R(COO^-)_x]_{ads}$ groups undergo oxidation under the thermal conditions of the precipitation process (T=100ºC), thus enabling the reduction of the auric complexes on HapNP surface to aurous species and mimicking the role of acetone dicarboxylic acid reported by Kumar et al[48]. Furthermore, the vicinity of the resulting aurous species will be an advantageous condition for the disproportionation reaction to proceed, towards Au^0 nucleation.

Although previous reports have shown that gold precipitation may take place on oxides pristine surfaces where O^- or OH^- are the protagonist surface species interacting with solution gold complexes[49-51], long precipitation times are however required (≥1h) as compared to the few minutes reported in this work. The used HapNPs thus behaved as a substrate that prompted the heterogeneous nucleation of AuNPs without the addition of any reducing agent like $NaBH_4$, one of the most used reagents for gold ions reduction[44]. Another method for depositing gold on the surface of Hap nanoparticles was reported by J.-D.Wang *et al*[52]: using urea as a precipitating agent, a gold precursor ($Au(OH)_3$) was precipitated which was later converted to metallic gold upon heat treatment at 350ºC. Therefore, as compared to that synthesis route the present method offers a straightforward way to produce metallic gold, exempting any precipitating agent or intermediate calcination step. The

carboxylic species attached to HapNP surface are thus a strategic tool for the "in situ" gold reduction and nucleation hence leading to AuNPs uniformly distributed on HapNPs facets, without the need of any additional surfactant for stabilization[19]. Being attached to HapNPs surfaces AuNPs are not prone to aggregation thereby eliminating potential drawbacks associated to aggregates.

Recent reports have covered the multiple functionalities recognised to AuNP some of which in a concerted manner may convey to a synergy of performances in the field of therapeutics[53,54]. In the present case the coupling of AuNp to HapNP imparts a SPR effect to the resulting composite nanostructure which could be further exploited for thermotherapy: AuNP are envisaged to empower HapNPs with hyperthermia ability for treating near-surface tumours or skin-type cancers where the laser requirements are less strict than for tumours located deep within bodily tissue for which a laser light in the near-infrared (NIR) region of the biological water window (650-900 nm) would be recomended[29]. Moreover HapNP can also behave as drug delivery systems (DDS) [55]due to their ability of adsorbing and releasing therapeutic drugs[55]. Endowing such DDS with a thermal response afforded by AuNP could open the possibility of customizing a HapNP-based DDS to a target of interest. It was reported that by adding a thermo-responsive coating to a DDS allows to use the induced thermal stimulus to trigger the drug delivery only at the local of interest[56], thus confining the drug effects to the unhealthy tissue while minimizing drug losses before the diseased cells are reached. Besides thermotherapeutic benefits, AuNP may also provide imaging capabilities as demonstrated in a recent study where the ability of gold nanoparticles to perform as a CT imaging contrast agent for tumour CT imaging was reported[54]. Therefore the hydroxyapatite based nanostructures (Hap-AuNPs) engineered in the present work offer promising characteristics for thermotherapeutic and imaging functionalities. The exploration of such attributes will warrant a large interest as it might expand the pool of applications of Hydroxyapatite beyond its well known medical use in hard tissue regeneration.

3.3- Interaction of Hap-AuNPs with human mesenchymal stem cells

As already pointed out, because of the similarity of Hap to the mineral phase of bone tissue and thus its natural bone affinity and biocompatibility, a range of bone tissue-related applications are envisaged for HapNP[26,27]. In a previous work, HapNP similar to those reported here proved to be non-toxic to MG63 osteoblastic cells regarding cell

viability/proliferation, F-actin cytoskeleton organization and apoptosis rate and, in addition, they increased the expression of ALP and BMP-2[23]. In order to assess the potential of the synthesized Hap-AuNPs for bone-related applications, the particles obtained after 5 min reaction time were selected to be cultured with human mesenchymal stem cells-bone marrow derived, due to their potential in bone regenerative approaches. HMSC were cultured in standard culture conditions, with the medium supplemented with ascorbic acid, because of its role in the synthesis of the bone collagenous extracellular matrix[57], but in the absence of any osteogenic inducer. Cell response of HMSC to the NPs was assessed for cell viability/proliferation and osteoblastic-related markers.

DNA content. The DNA content of control cultures (absence of NPs) increased throughout the culture time. Comparatively, exposure to HapNP or Hap-AuNPs (1 - 500 μg/ml) did not result in any evident effects. As the DNA content reflects the number of cells present on the cultures, this observation suggests that the two nanoparticles did not interfere in the proliferation of HMSC. Results are shown in Figure 7a.

Cellular viability. The viability of HMSC grown with the NPs was assessed by the MTS reduction assay and the LDH release assay. Mostly, results for the MTS assay, based on the reduction ability of cell mitochondrial dehydrogenases by viable cells, showed similar values for the control and NPs-exposed cultures, Figure 7b. However, cultures exposed to 10 and 100 μm/ml NPs for 7 days displayed a slight increase in the metabolic activity, which attained statistical significance for Hap-AuNPs nanoparticles. On the other hand, cultures treated with 500 μg/ml HapNP or Hap-AuNPs, during 7 days, displayed a slight decrease, suggesting lower reduction ability. On the LDH assay, Figure 7c, the LDH released to the medium throughout the culture time revealed low values on the control cultures and those exposed to 1–100 μg/ml NPs, suggesting minimal deleterious effects on the cell membrane integrity; however, an increase was seen in the presence of the higher nanoparticles levels (500 μg/ml), following 3 and 7 days exposure, suggesting a somewhat compromised cell viability; still, the increase on the percentage of LDH leakage was only around 9% upon 7-days exposure, compared to ~6.5% in the control cultures. These observations are in line with that observed in MTS assay.

F-actin cytoskeleton. Observation of the cultures under CLSM, following staining for F-actin cytoskeleton and nucleus counterstaining, corroborated the low toxicity profile of HapNP and Hap-AuNPs particles. The cell adhesion to the culture substrate and the

subsequent cytoplasmic expansion were similar in the absence and in the presence of the nanoparticles. At day 1, cells displayed an elongated morphology, establishing elementary cell-to-cell contacts. Following, a high cell growth rate was noticed; at day 3, areas of high cell density were already visualized and, at day 7, cultures showed confluent zones with continuous cell multilayers. Cells exhibited a well-organized F-actin cytoskeleton, with intense staining at the cell boundaries, prominent nucleus and on-going cell division, signs of mechanical integrity and healthy behaviour. Representative images are shown in Figure 8, for the cultures exposed to 100 μg/ml NPs. The F-actin cytoskeleton, which is highly concentrated just beneath the plasma membrane, provides structural stability and elasticity to the cell undergoing substrate adaptation, but it is also a key player in the cellular mechano-transduction mechanisms modulating complex signalling pathways, such as Rho family GTPases, which affects the overall cell behaviour[58]. Thus, these results further support the cytocompatibility of HapNP and Hap-AuNPs towards mesenchymal stem cells.

Osteoblastic gene expression. Additionally, gene expression by reverse-transcription polymerase chain reaction (RT-PCR) was performed to investigate osteogenic signal expression in the presence of HapNP and Hap-AuNPs nanoparticles (100 μg/ml), Figure 9a. Hap-AuNPs nanoparticles greatly induced the expression of Runx2 (~100%), compared to the slight increase observed with HapNP particles. This is an interesting finding, as Runx2 is the earliest transcription factor for the osteogenic differentiation pathway and, in addition, it is a master regulator for the expression of multiple late stage genes, being determinant for osteoblastic differentiation and bone formation[57]. Both particles showed a trend for an increase in the expression of Col 1, the main component of the bone extracellular matrix, synthesized during the proliferative stage of the osteoblastic differentiation pathway[57]. Of interest, Hap and Hap-AuNPs particles had a significant impact in the expression of ALP, with more than a 4-fold increase in the expression level of this early osteoblastic differentiation marker. Expression of osteocalcin, a late osteoblastic differentiation marker, with a role in the regulation of crystal growth[57], was not particularly affected by HapNP or Hap-AuNPs particles. This suggests that these particles appear to not interfere in the regulatory mechanisms of the matrix mineralization. Regarding the expression of OPG, a key molecule in the interplay between osteoblasts and osteoclasts during bone remodelling, it was not affected by Hap but was slightly reduced in the presence of Hap-AuNPs particles.

ALP activity. Cultures exposed to HapNP and Hap-AuNPs particles (100 μg/ml) were also assessed for ALP activity. In line with the increased gene expression for this enzyme, ALP activity was greatly induced by the two nanoparticles. The inductive effect was observed already after 1 day exposure, but greatly increased at day 3 (~150%) and day 7 (~80%) (Figure 9b). ALP, a hallmark of osteoblastic differentiation, is synthesized during the early matrix formation and maturation period. This enzyme has an essential role in the onset of matrix mineralization, by providing phosphate ions which, together with calcium ions, ensure the chemical conditions for the osteoblastic-mediated mineral deposition[57].

Literature reports on the interaction of osteoblast lineage cells with Hap nanoparticles show a great variability of results, which is expected considering the wide versatility and diversity of the physicochemical properties of the tested particles, the cell system and the experimental protocols[23,59-63]. However, regarding the present HapNP, the observed cell response is in line with previous reports showing low cytotoxicity of Hap nanoparticles towards osteoblastic cells, and also their ability to modulate cell proliferation and differentiation events. Upon exposure to HapNP, increased proliferation was found in bone marrow-derived mesenchymal stem cells[63] and enhanced osteoblastic differentiation features was also observed for these cells[59, 63], and also for the osteoblastic cell lines hFOB 1.19[62] and MG63[23]. On the other hand, cytotoxicity/biocompatibility studies involving AuNPs coupled with hydroxyapatite are rare or even inexistent. About AuNPs, the osteoblastic cell response also showed variable results. In the murine preosteoblast cell line MC3T3-E1, AuNP did not affect cellular viability[64], and in another study they promoted their viability and osteogenic differentiation, depending on the particle size[65]. In mesenchymal stem cells, AuNPs promoted the viability and osteogenic differentiation[66], but they were also reported to be toxic to these stem cells, depending on the particle size[67]. AuNp aggregation state also influences the cellular uptake and cytotoxicity as reported for different cell types[68,69] though not following a simple rule of thumb as aggregated AuNP may result in cytotoxicity or favour cell growth depending on the aggregate size which in turn conditions its internalization[68]. The conflicting results could also arise from the variability of the used toxicity assays, cell systems, and nanoparticles chemical/physical properties; additionally, the dosing parameters and the exposure time to AuNPs vary, making it difficult to compare. In the present work, the synthesized Hap-AuNPs showed low cytotoxicity and this may reflect the use of a system where AuNP of very low size are fixed

to a HapNP template and thus inhibited to undergo agglomeration. Hap-AuNPs also evidenced the ability to enhance early phenotype markers for osteogenic differentiation in HMSC, i.e. ALP expression and activity. Further, of relevance, is the great increase in the expression of Runx2, pointing to a higher commitment of the mesenchymal stem cells towards the osteogenic lineage in the presence of these particles. Regarding this, it has been reported that AuNPs are able to activate the p38 MAPK signaling pathway in MSCs, which leads to the up-regulation of the osteogenic master transcriptio factor Runx2, driving MSCs to differentiate toward osteoblast cells[66].

The promise of AuNP for many different biological applications has led to a strong interest in their cellular and tissue compatibility. Regarding this, the response of the synthesized Hap-AuNPs towards mesenchymal stem cells seems to substantiate interesting features in bone related applications, from imaging and drug delivery to regenerative approaches. However, their ability to affect the fate of mesenchymal stem cells, i.e. by enhancing the osteogenic differentiation pathway, should also be carefully considered in bone-related and other biomedical applications.

4-Conclusions

Gold nanoparticles (AuNPs) were successfully synthesized on the surface of Hydroxyapatite nanoparticles (HapNP). The presence of organic species containing carboxylate groups on HapNP surface left by the synthesis process of the HapNP themselves was a key condition for enabling *in situ* ionic gold reduction to metal gold which resulted in spherical AuNPs with a diameter of few nanometers. The presence of nanometric gold on the resulting composite particle (Hap-AuNPs) imparts SPR effect to the final particles which may be further explored for imaging and therapy purposes. Interaction of Hap-AuNPs with mesenchymal stem cells converged to confirm the nanoparticles cytocompatiblity and also their enhancing osteoblastic differentiation properties. This profile substantiates Hap-AuNPs as promising materials for bone-related applications as well.

Acknowledgements

This work was financed by FEDER, via ‘‘Programa Operacional Factores de Competitividade – COMPETE’’, FCT – ‘‘Fundação para a Ciência e a Tecnologia’’, PEst-C/CTM/LA0011/2011, and FMDUP. The authors are grateful to the Portuguese Electronic Microscopy Network also supported with FCT funds. CLSM observation was performed at Advanced Light Microscopy, IBMC, University of Porto (IBMC.INEB) under the responsibility of Dr. Paula Sampaio.

References

1 Y. Xia, *Nat. Mater.*, 2008, **7**, 758-760.
2 Y. Zhang, Y. Guo, Y. Xianyu, W. Chen, Y. Zhao and X. Jiang, *Adv. Mater.*, 2013, **25** (8), 3802-3819.
3 E. C. Dreaden, A. M. Alkilany, X. Huang, C. J. Murphy and M. A. El-Sayed, *Chem. Soc. Rev.*, 2012, **41 (7)**, 2740-2779.
4 G. von Maltzahn, J.-H. Park, K. Y. Lin, N. Singh, C. Schwöppe, R. Mesters, W. E. Berdel, E. Ruoslahti, M. J. Sailor & S. N. Bhatia, *Nat. Mater.*, 2011,**10**, 545-552.
5 G. von Maltzahn, J.-H. Park, A. Agrawal, N. K. Bandaru, S. K. Das, M. J. Sailor and S. N. Bhatia, *Cancer Res.*, 2009, **69(9)**, 3892-3900.
6 K. Kim, D. Dean, A. Lu, A. G. Mikos and J. P. Fisher, *Acta Biomater.*, 2011, **7 (3)**, 1249-1264.
7 M. Patel, K. J. Patel, J. F. Caccamese, D. P. Coletti, J. J. Sauk and J. P. Fisher, *J. Biomed. Mater. Res. A*, 2010, **94A (2)**, 408-418.
8 S. Yang, D. Wei, D. Wang, M. Phimphilai, P. H. Krebsbach and R. T. Franceschi, *J. Bone Miner. Res.*, 2003,**18(4)**, 705-715.
9 M. J. Olszta, X. Cheng , S.S.Jee, R. Kumar, Y.-Y. Kim, M. J. Kaufman, E. P. Douglas and L. B. Gower, *Mat. Sci. Eng. R*, 2007, **58 (3-5)**, 77-116.
10 A. Dey, P. H. H. Bomans, F. A. Müller, J. Will, P. M. Frederik, G. de With & N. A. J. M. Sommerdijk, *Nat. Mater.*, 2010, **9**, 1010-1014.
11 L. M. Liz-Marzán, M. Giersig and P. Mulvaney, *Langmuir*, 1996, **12 (18)**, 4329-4335.
12 S. Aryal, R. B. K.C., S. R. Bhattarai, P.Prabu and H.Y. Kim, *J.Mater.Chem.*, 2006, **16**, 4642-4648.
13 Y. Ding, J. Liu, H. Wang, G. Shen and R. Yu, *Biomaterials*, 2007, **28 (12)**, 2147-2154.
14 T. P. Sastry, J.Sundaraseelan, K.Swarnalatha, S. S. L. Sobhana, M. U. Makheswari, S. Sekar and A. B. Mandal, *Nanotechnology*, 2008, **19**, 245604.

15 Y. Gupta, G.N.Mathur and S. Verma, *Bioorg. Med. Chem. Lett.*, 2006, **16 (2)**, 363-366.
16 S. Arumugan, A. M. Rajam, N.Natarajan, U. Rao, C.Rose and T.P.Sastry, *J. Biomed. Nanotechnol.*, 2006, **2**, 46-52.
17 K. C. R. Bahadur, S. Aryal, N. Bhattarai and H.Y.Kim, *Scripta Mater.*, 2006, **54(12)**, 2029-2034.
18 J. Turkevich, P.C. Stevenson and J. Hillier, *Discuss. Faraday Soc.*, 1951, **11**, 55-75.
19 J. B. Hannon, S. Kodambaka, F. M. Ross and R. M. Tromp, *Nature*, 2006, **440**, 69-71.
20 Y. Wang, S. Zhang, K. Wei, N. Zhao, J. Chen and X. Wang, *Mater. Letter*, 2006, **60 (12)**, 1484-1487.
21 C.R.Kothapalli, M.Wei, R.Z.Legeros and M.T.Shaw, *J. Mater. Sci.- Mater. M.*, 2005, **16**, 441-446.
22 H. Arce, M. L. Montero, A. Sáenz, V. M. Castaño, *Polyhedron*, 2004, **23 (11)**, 1897-1901.
23 C. Santos, P. S. Gomes, J. A. Duarte, R. P. Franke, M. M. Almeida, M. E. V. Costa and M. H. Fernandes, *J. Roy. Soc. Interface*, 2012, **9**, 3397-3410.
24 M.A.Martins, C.Santos, M.M.Almeida and M.E.V.Costa, *J Colloid Interf. Sci.*, 2008, **318**, 210-216.
25 S. P. Garcia and S. Semancik, *Chem.Mater.*, 2007, **19 (16)**, 4016-4022.
26 K. Fox, P. A. Tran and N. Tran, *ChemPhysChem*, 2012, **13(10)**, 2495-2506.
27 H. Zhou and J. Lee, *Acta Biomater.*,2011,**7**, 2769-2781.
28 S.Link and M.A. El-Sayed, *J.Phys.Chem B*, 1999,**103 (40)**, 8410-8426.
29 P. K. Jain, X. Huang, I.H. El-Sayed, M.A.El-Sayed, , *Plasmonics*, 2007,**2(3)**,107-118.
30 P. Schneider, *Appl. Catal. A-Gen.*, 1995, **129**, 157-165.
31 T. Mosmann, *J. Immunol. Methods*, 1983, **65**,55-63.
32 T. Decker and M.-L. Lohmann-Matthes, *J. Immunol. Methods*, 1988, **115**, 61-69.
33 N. H. d. Leeuw and J. A. L. Rabone, *CrystEngComm*, 2007,**9**, 1178-1186.
34 B. A. J. Noordover, R. Duchateau, R. A. T. M. van Benthem, W. Ming and C. E. Koning, *Biomacromolecules*, 2007, **8**, 3860–3870.
35 D. Jiang and J. Zhang, *Curr. Appl. Phys.*, 2009,**9**, S252–S256.
36 S. Bednarz, M. Lukasiewicz, W. Mazela, M. Pajda and W. Kasprzyk, *J. Appl. Polym, Sci,*, 2011,**119**, 3511-3520.
37 D. Wyrzykowski, E. Hebanowska, G. Nowak-Wiczk, M. Makowski, L. Chmurzyński, *J. Therm. Anal. Calorim.*, 2011, **104**, 731-735.
38 T. B. Mostafa, H. F. Naguib, M. W. Sabaa and S. M. Mokhtar, *Polym. Int.*, 2005,**54**, 221-225.

39 G. D. Cody, N. Z. Boctor, R. M. Hazen, J. A. Brandes, H. J. Morowitz and H. S. Yoder Jr, *Geochim. Cosmochim. Ac.*, 2001,**65 (20)**, 3557-3576.

40 S. R. Qiu, A. Wierzbicki, C. A. Orme, A. M. Cody, J. R. Hoyer, G. H. Nancollas, S. Zepeda, J. J. De Yoreo, *PNAS*, 2004,**101**, 1811-1815.

41 D. Holzmann, D. Holzinger, G. Hesser, T. Schmidt and G. Knör, *J. Mater Chem.*, 2009,**19**, 8102-8106.

42 C. J. Murphy, A. M. Gole, J. W. Stone, P. N. Sisco, A. M. Alkilany, E. C. Goldsmith and S. C. Baxter, *Accounts Chem. Res.*, 2008, **41**, 1721-1730.

43 F. Caruso, M. Spasova, V. Salgueiriño-Macieira and L. M.Liz-Marzán,*Adv. Mater.*, 2001, 13, 1090-1094.

44 Z. Wang, S. Zong, J. Yiang, J. Li,Y.Cui *Biosens. Bioelectron.*, 2011,**26(6)**, 2883-2889.

45 M. Bradley and B. S. Garcia-Risueño, *J. Colloid Interf.* Sci, 2011, **355 (2)**, 321-327.

46 D.-Q. Yang, M. Meunier and E. Sacher, *J. Appl. Phys.*, 2004,**95**, 5023-5026.

47 K.van Werde, D. Mondelaers, G.Vanhoyland, D.Nelis, ~~B.~~ M.K.van Bael, J.Mullens and L.C. van Poucke, *J. Mater. Sci.*, 2002,**37**, 81-88.

48 S. Kumar, K.S.Gandhi and R.Kumar, *Ind.Eng.Chem.Res.*, 2004,**46(10)**, 3128-3136.

49 S. Ivanova, C. Petit and V. Pitchon, *Applied Catalysis A: General*, 2004, 267, 191–201.

50 F. Moreau, G. C. Bond and A. O. Taylor, *Journal of Catalysis*, 2005, **231 (1)**, 105–114.

51 K. Zhao, B. Qiao, J. Wang, Y. Zhang and T. Zhang, *Chem. Commun.*, 2011, **47**, 1779–1781.

52 J.-D. Wang, J.-K. Liu, Y. Lu, D.-J. Hong, X.-H. Yang, *Mater. Res. Bull.*, 2014, **55**, 190–195.

53 A. J. Mieszawska, W. J. M. Mulder, Z. A. Fayad and D. P. Cormode, Mol. Pharmaceutics, 2013, **10 (3)**, 831−847.

54 J. Park, J. Park, E. J. Ju, S. S. Park, J. Choi, J. H. Lee, K. J. Lee, S.H. Shin, E. J. Ko, I. Park, C. Kim, J. J.H. Wang, J. S. Lee, S. Y. Song, S.-Y. Jeong and E. K. Choi, *Journal of Controlled Release*, 2015,**207**, 77–85.

55 T. Scharnweber, C. Santos, R.-P. Franke, M. M. Almeida and M. E. V. Costa, *Molecules*, 2008, **13**, 2729-2739.

56 Y. Liu, X. Cao, M. Luo, Z. Le and W. Xu, J. *Colloid Interf. Sci.*, 2009, **329**(2), 244–252.

57 L. G. R. a. T. J. M. John P. Bilezikian. *Principles of Bone Biology*. Vol. 1 (Academic Press, 2008).

58 I. Titushkin, S. Sun, J. Shin M. Cho, *J. Biomed. Biotechnol.*, 2010, **2010**,1-14.

59 R. Gonzalez-McQuire, D. W. Green, K. A. Partridge, R. O. C. Oreffo, S. Mann and S. A. Davis, *Adv. Mater.*, 2007, **19**, 2236-2240.

60 Y. Cai and R. Tang, J. Mater. Chem., 2008,**18**,3775-3787.

61 Z. Shi, X. Huang, Y. Cai, R. Tang and D. Yang, *Acta Biomater.*, 2009, **5 (1)**, 338-345.

62 J. L. Xu, K. A. Khor, J. J. Sui, J. H. Zhang and W. N. Chen, *Biomaterials*, 2009, **30 (29)**, 5385-5391.

63 Y. Liu, G. Wang, Y. Cai, H. Ji, G. Zhou, X. Zhao, R. Tang and M. Zhang, *J. Biomed. Mater. Res. A*, 2009, **90A**, 1083-1091.

64 T. Mustafa, F. Watanable, W. Monroe, M. Mahmood, Y. Xu, L. Saeed, A. Karmakar, D. Casciano, S. Ali and A. Biris, *J. Nanomed. Nanotechnol.*, 2011 **2(6)**,118-124.

65 D.D. Liu, J.C. Zhang, C.Q. Yi and M.S. Yang, *Chinese Sci. Bull.*, 2010, **55**, 1013-1019.

66 C. Yi, D. Liu, C.-C. Fong, J. Zhang and M. Yang, *ACS Nano*, 2010, **4**, 6439-6448.

67 J.-H. Fan, W.-T. Li, W.-I. Hung, C.-P. Chen and J.-M. Yeh, *Biomed. Eng. - App. Bas. C.*, 2011, **23**, 141-152.

68 W. Cui, J. Li, Y. Zhang, H. Rong, W. Lu and L. Jiang, *Nanomedicine: Nanotechnology, Biology, and Medicine*, 2012, **8 (1)**, 46–53.

69 J. A. Yang, S. E. Lohse and C. J. Murphy, *Small*, 2014,**10**, 1642-1651.

Table 1 – Primers used on RT-PCR analysis.

Gene	Forward primer	Reverse primer
GAPDH	CAGGACCAGGTTCACCAACAAGT	GTGGCAGTGATGGCATGGACTGT
Runx2	CAGTTCCCAAGCATTTCATCC	TCAATATGGTCGCCAAACAG
COL1	TCCGGCTCCTGCTCCTCTTA	ACCAGCAGGACCAGCATCTC
ALP	ACGTGGCTAAGAATGTCATC	CTGGTAGGCGATGTCCTTA
OC	CACTCCTCGCCCTATTG	CCCACAGATTCCTCTTCT
OPG	AAGGAGCTGCAGTAGGTCAA	CTGCTCGAAGGTGAGGTTAG

Captions

Figure 1- Optical pictures of hydroxyapatite nanoparticles: (a) as synthesized at 180ºC (HapNP) and after being submitted to gold precipitation (Hap-AuNP) during (b) 5min, (c) 10min and (d) 20min. The particle color evolution denotes the presence of metallic gold.

Figure 2- X-ray diffraction patterns of hydroxyapatite nanoparticles: (a) as produced at 180ºC (HapNP) and after being submitted to gold precipitation (Hap-AuNP) during (b) 5min, (c) 10min and (d) 20min. The peak detected at 2θ ~ 38º is assigned to metallic gold.

Figure 3- FTIR spectra of (a) HapNP synthesized at 180ºC ( ) and its evolution with metallic gold precipitation after 5min ( ), 10 min ( ) and 20 min ( ); (b) the 1200-1900 cm^{-1}spectral region is amplified.

Figure 4- (a) TEM images showing the elongated prismatic shape of HapNP. (b) The hexagonal base of prismatic particles is confirmed on a particle top view.

Figure 5- HRTEM images of Hap-AuNPs collected after two different precipitation times: (a) 5 min and (b) 20 min. The particles are spotted with nanosized dark dots of metallic gold (AuNP) which were precipitated on HapNP facets. (c) AuNP size distribution precipitated after 5 and 20 min.

Figure 6- UV/Vis spectra of (a) HapNP synthesized at 180ºC and after reacting with gold solution (Hap-AuNPs) during (b) 5 min and (c) 20 min. The characteristic surface plasmon resonance band of gold nanoparticles is clearly observed at ~552 nm for the Hap-AuNPs.

Figure 7- (a) DNA content, (b) MTS reduction and (c) LDH leakage of HMSC cultured for 1, 3 and 7 days in the presence of HapNPs and Hap-AuNPs, 1 – 500 μg/ml. NPs did not interfere with the cellular proliferation and metabolic activity in the range 1 - 100 μg/ml, but exposure to 500 μg/ml caused a slight decrease in the cellular viability.*Significantly different from control (absence of NPs).

Figure 8- Representative Confocal Laser Scanning Microscopy images of HMSC cultured for 3 and 7 days in the presence of HapNPs and Hap-AuNPs, 100 μg/ml. Cultures were stained for the cytoskeleton (green) and nucleus (red). Cellular morphology and organization of the cell layer were similar in control and NPs-exposed cultures. Bar: 50 μm.

Figure 9- (a) Gene expression and (b) ALP activity of HMSC cultured in the presence of HapNPs and Hap-AuNPs, 100 μg/ml; (a) cultures with 3 days; (b) cultures with 1, 3 and 7 days. *Significantly different from control (absence of NPs). Hap-AuNPs caused a significant increase in the expression of Runx2, and both NPs increased ALP expression and activity.

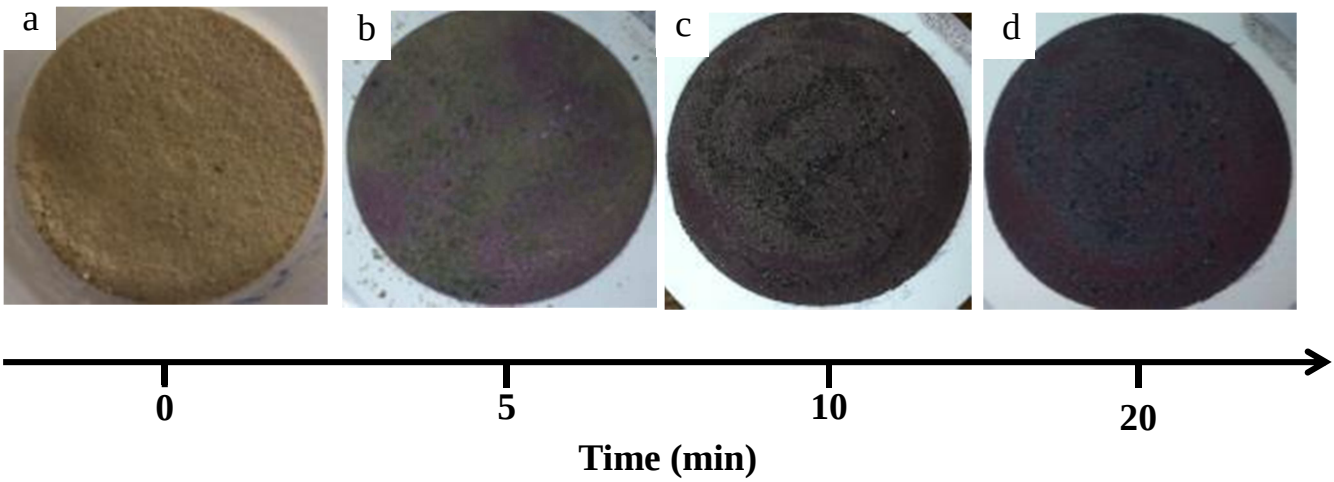

Figure 1

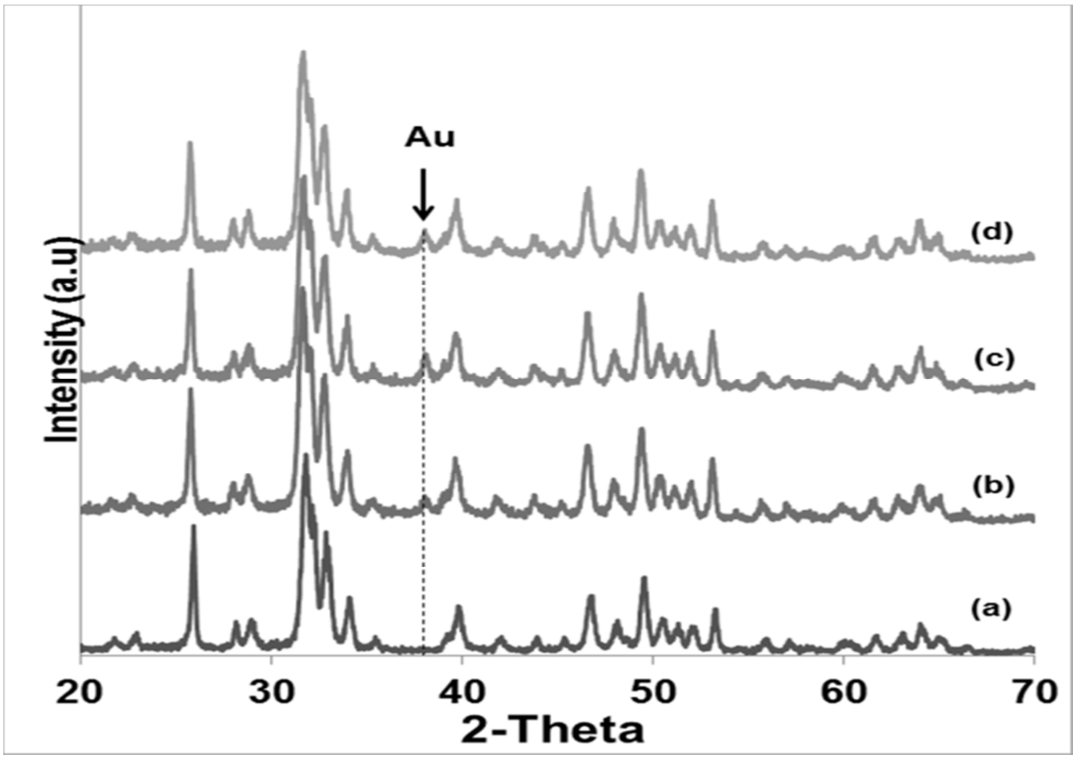

Figure 2

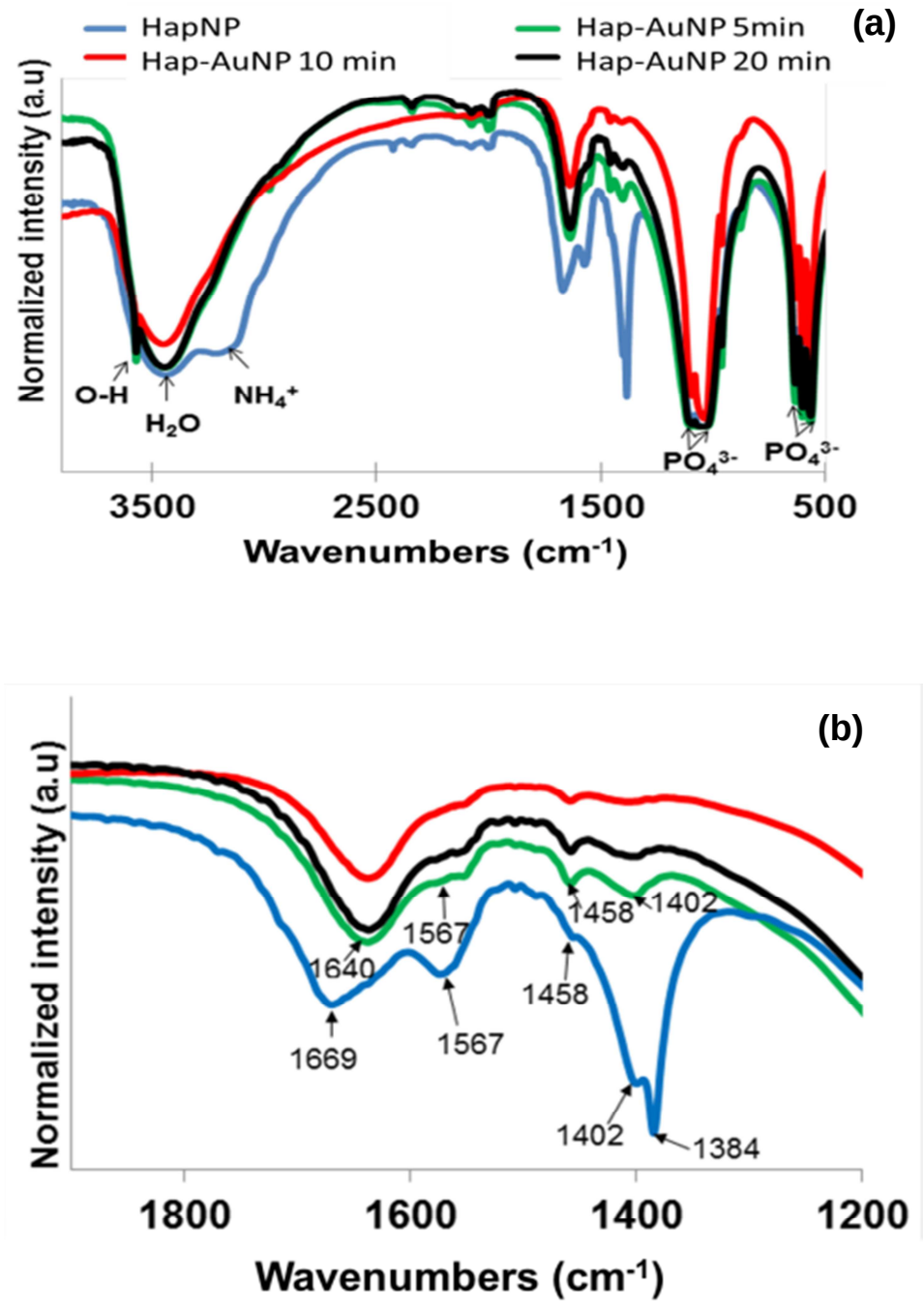

Figure 3

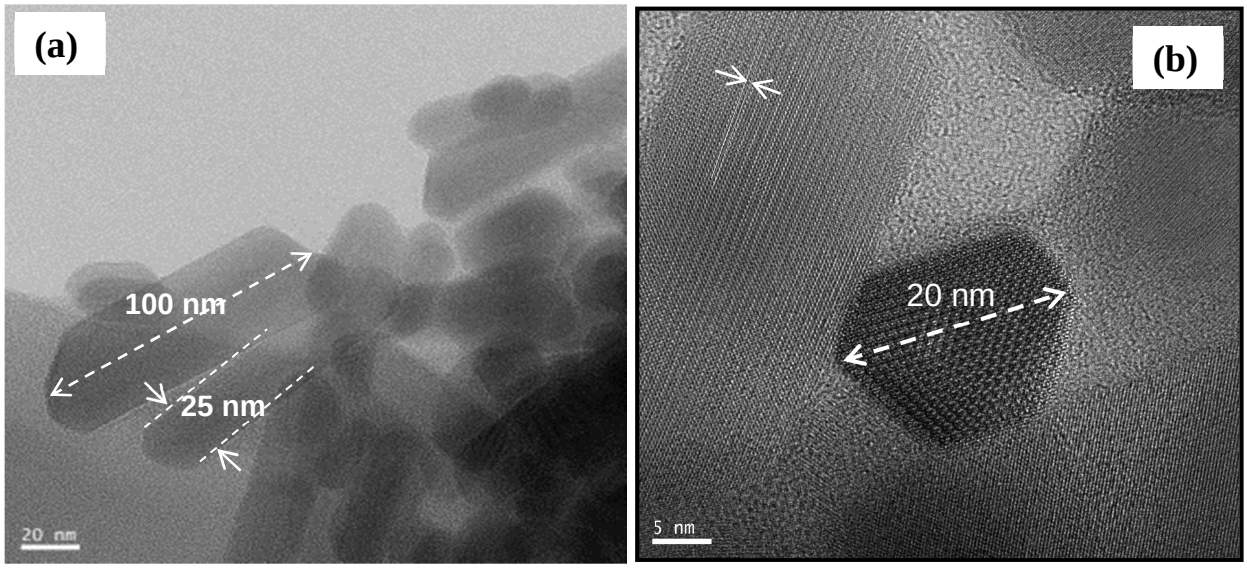

Figure 4

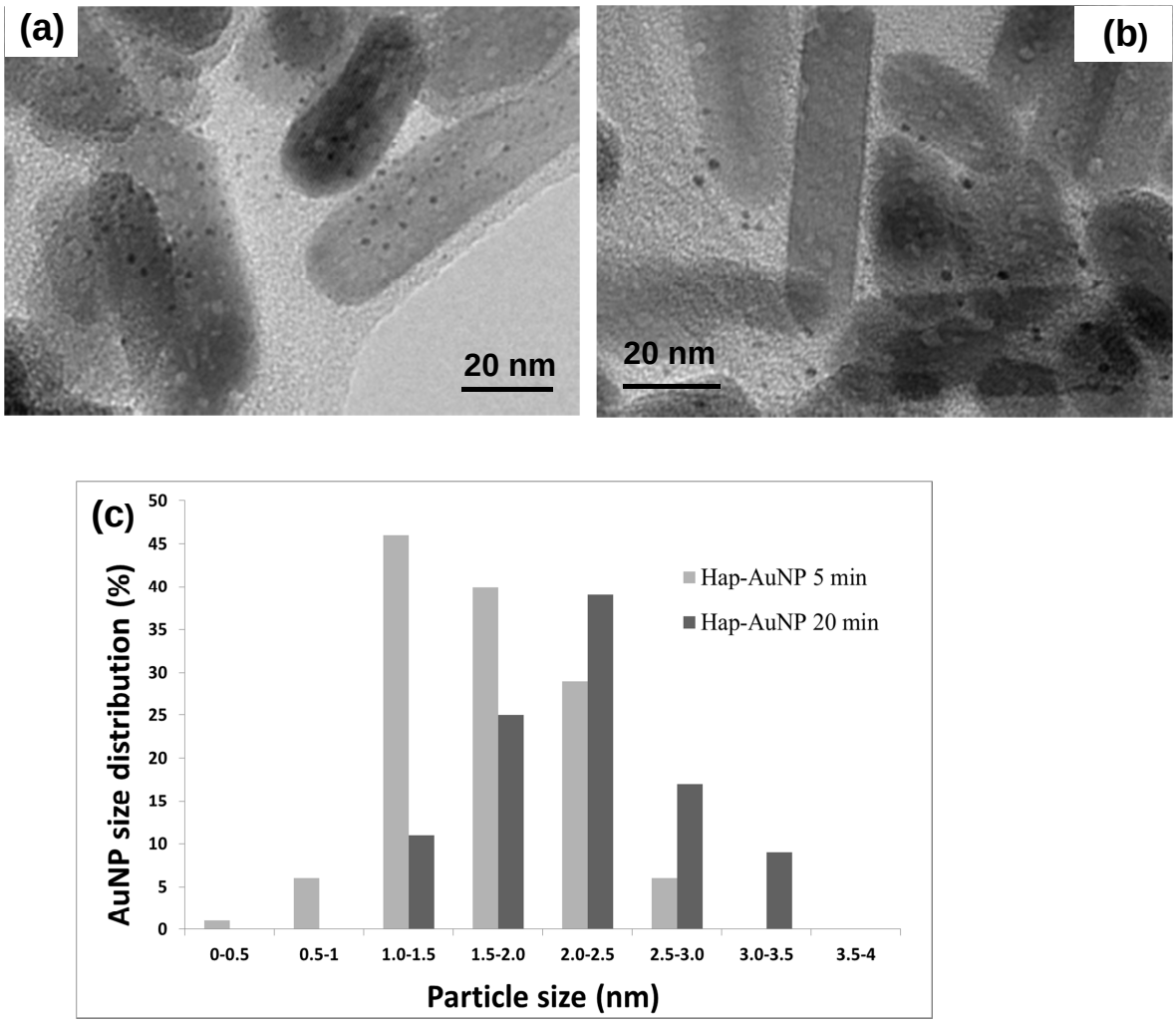

Figure 5

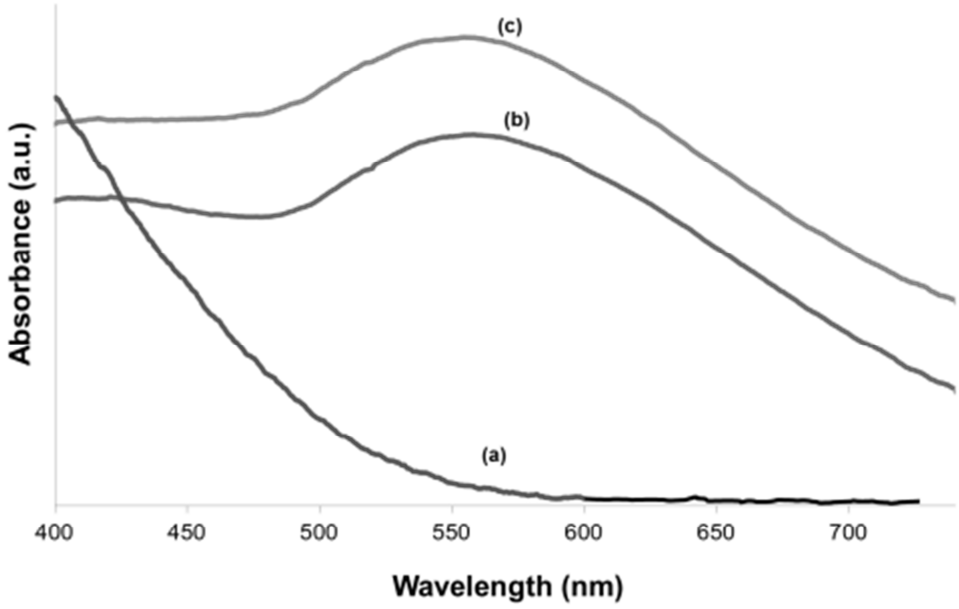

Figure 6

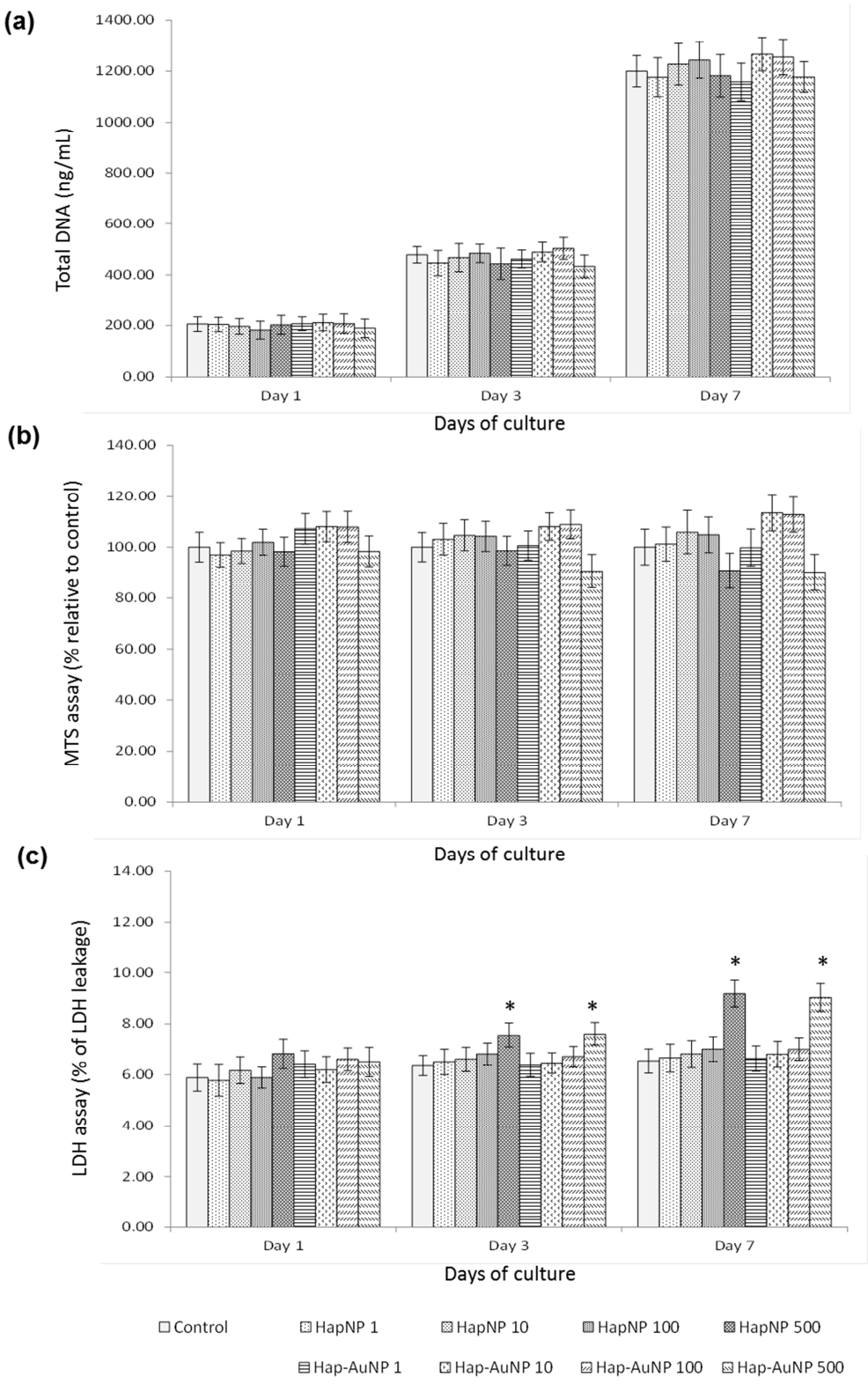

Figure 7

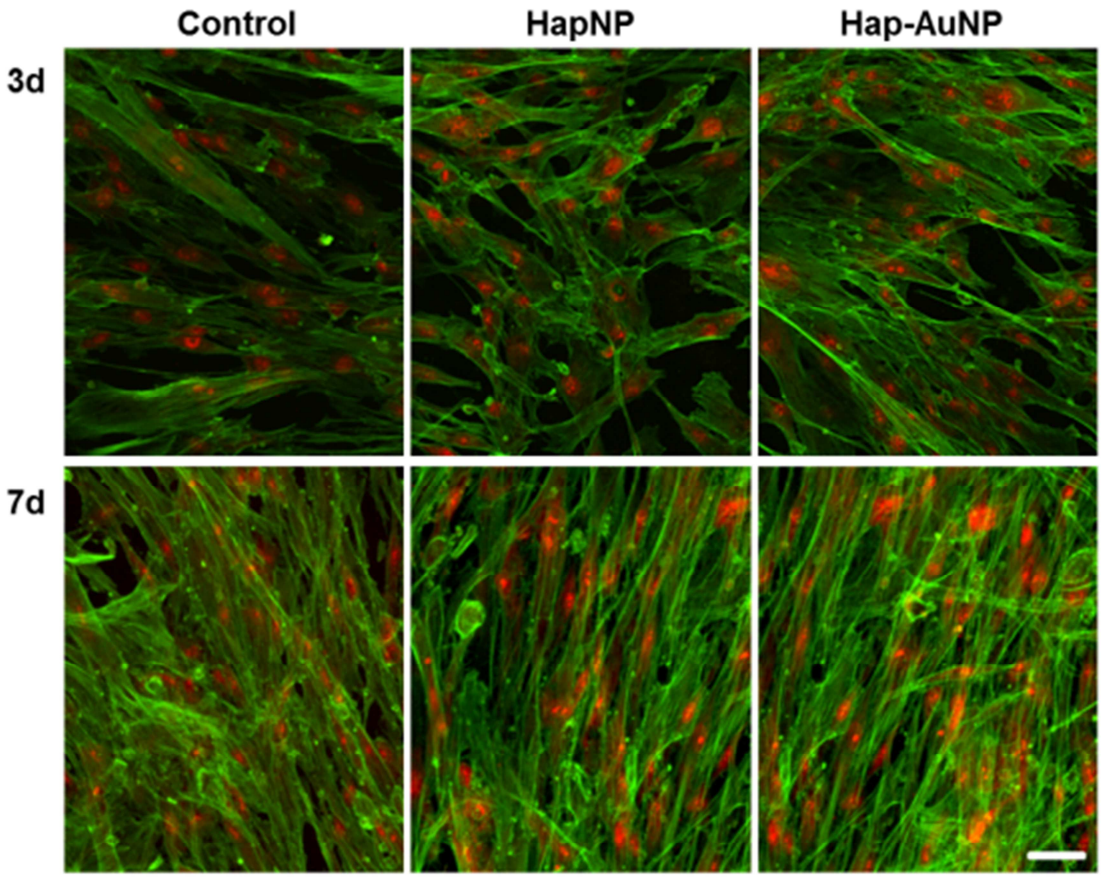

Figure 8

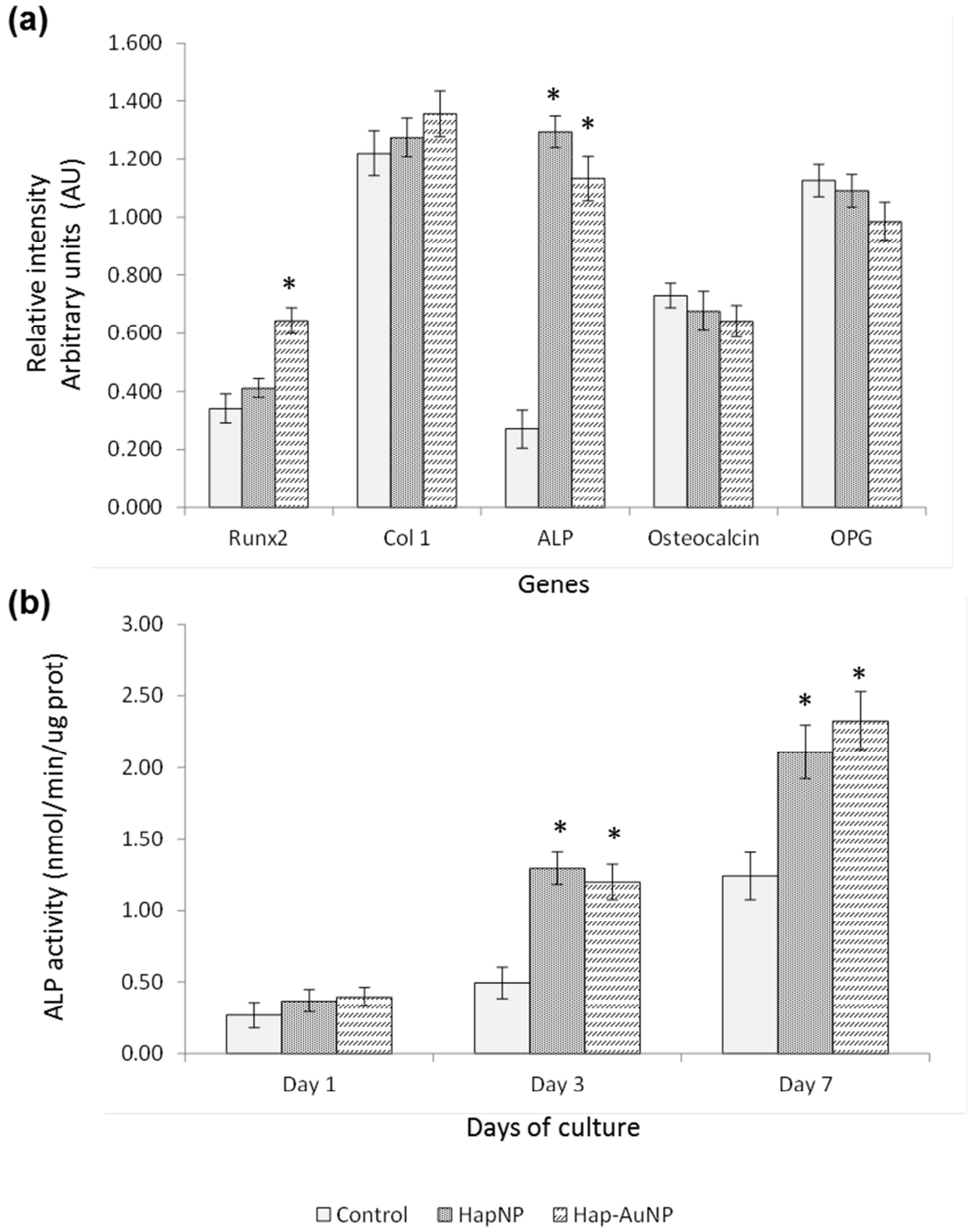

Figure 9